Unraveling the Salvinia paradox: design principles for submerged superhydrophobicity

M. Amabili[1], A. Giacomello[1,*], S. Meloni[2], & C.M. Casciola[1]

1. Dipartimento di Ingegneria Meccanica e Aerospaziale, Università di Roma "La Sapienza", Rome, Italy

   E-mail: alberto.giacomello@uniroma1.it

2. Institute of Chemical Sciences and Engineering, École Polytechnique Fédérale de Lausanne, Lausanne, Switzerland

keywords: superhydrophobicity; Salvinia effect; submerged surfaces; Cassie-Wenzel transition; rare events methods.

Inspired by nature[1], the study of superhydrophobicity has flourished in the last two decades allowing for an improved control of the wetting properties of surfaces of technological interest[2,3]. In particular, submerged superhydrophobicity is emerging as a means to reduce drag and prevent biofouling: such applications require robust gas-trapping inside surface asperities. Here, we focus on the *Salvinia effect*[4], assessing both via free energy atomistic simulations and via macroscopic capillarity theory the role of the complex morphology of this water fern (Figure 1a) in stabilizing an air layer underwater. Our analysis shows that the Salvinia effect is in essence determined by the pinning of the contact line and by the characteristic size of surface roughness. Simple design criteria for stable submerged superhydrophobicity are devised, consolidating the different approaches[5–7] within a common probabilistic framework.

1

Most applications of superhydrophobicity to date have concentrated on drops deposited on surfaces, both statically and dynamically. On the other hand, there is a growing interest in the properties of submerged surfaces entrapping gas[8–10]: in this case, superhydrophobicity is a means to reduce the liquid-solid contact which, in turn, diminishes drag[11–13] and prevents (bio)fouling. Given their relevance for global industry and transportation, even small improvements in the fuel efficiency and maintenance costs of watercrafts and marine structures could have a significant impact on society[14,15]. For submerged applications the central question is the resistance and durability of the gas pockets to pressure variations. In fact, the common-ground of superhydrophobicity is the underlying "suspended" Cassie state in which gas pockets are trapped within surface asperities. Depending on the external conditions, however, superhydrophobicity may break down in the fully wet Wenzel state (Figure 1c).

The Lotus leaves have played a major role in inspiring the design of drop-repellent surfaces[1]. Moving towards submerged applications requires a new vegetable Muse: a promising candidate is the *Salvinia molesta* (Figure 1a), because of its superior vapor trapping capabilities[4,16].

The gas entrapped within surface asperities can be either air or the vapor phase coexisting with the liquid: albeit the partial pressure of the other gases facilitates the Cassie state, their presence is not a requirement for (meta)stable superhydrophobicity[18] (see *Supporting Information* for additional details on the role of dissolved gases). The entrapped gas may be lost through different mechanisms, analyzed in detail below, determining the failure of superhydrophobicity:

1. mechanical destabilisation of the Cassie state, e.g., due to an increase in the pressure (the *spinodal* for the Cassie-Wenzel transition);

2. *thermally activated* Cassie-Wenzel transition; this process is much slower than the spinodal one;

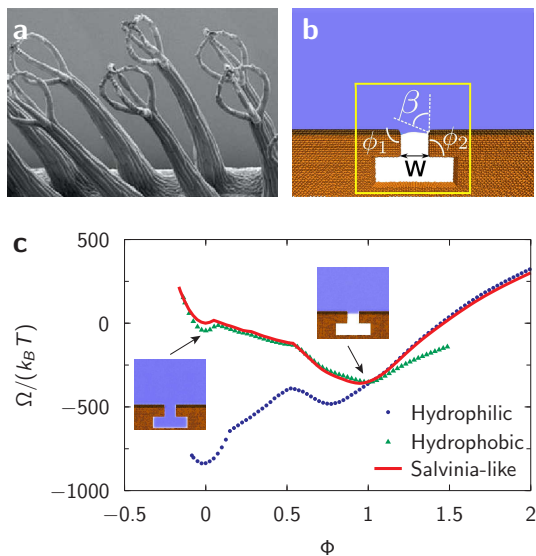3. gas loss in the liquid through *thermally activated* nucleation of bubbles

Figure 1: a) SEM micrograph of a Salvinia molesta leaf showing the egg-beater hairs (adapted from [4]). b) Atomistic Salvinia-like system used in RMD simulations. The fluid is represented in blue, the hydrophilic layer in dark brown, and the hydrophobic interior in light brown. No additional gas is present ($P_g = 0$). The yellow lines define the box for the atom count collective variable z [17]. c) Free energy profiles at $\Delta P \approx 0$ as a function of the filling level $\Phi \equiv (z_W - z)/(z_W - z_C)$ for the hydrophobic system (blue dots), the hydrophilic one (green triangles), and the Salvinia-like one (red line). z_W (z_C) is computed in the Wenzel (Cassie hydrophobic) state, shown in the insets for the Salvinia-like case. Thus, for the three chemistries, $\Phi = 0$ corresponds to the Wenzel state, $\Phi \sim 1$ to the Cassie state, and $\Phi > 1$ to a vapor bubble.

(at pressures below two-phase coexistence);

4. *spinodal* nucleation of bubbles (at pressures much below two-phase coexistence);

5. air dissolution in the liquid [19].

In order to rationalize these different scenarios and quantify the "robustness" of superhydrophobicity we compute the probability to find the system in a generic macroscopic state z. This probability $p(z; P, T)$ crucially depends on the thermodynamic conditions (pressure P and temperature T) and is usually expressed in a logarithmic scale and in units of the thermal energy – the so-called

Landau free energy Ω:

$$p(z; P, T) = \exp\left(-\frac{\Omega(z; P, T)}{k_B T}\right) , \qquad (1)$$

where z is a variable characterizing the macroscopic state of the system (here, the advancement of the Cassie-Wenzel transition) and k_B is the Boltzmann constant. When the free energy landscape $\Omega(z; P, T)$ is rugged, its local minima correspond to highly probable (meta)stable states, e.g., the Cassie and Wenzel states in the 1D landscape of Figure 1c.

The main pieces of information that can be extracted from $\Omega(z; P, T)$ are the free energy difference between any two states and the free energy barriers $\Delta\Omega^\dagger$. In particular, the difference between two minima in the free energy measures the relative probability of two (meta)stable states; for the case of the Cassie-Wenzel transition, $\Omega_C - \Omega_W = -k_B T \ln(p_C/p_W)$. The maximum (*transition state*) separating two minima defines two free energy barriers, a "forward" and a "backward" one: $\Delta\Omega^\dagger_{CW} \equiv \Omega_{\text{ts}} - \Omega_C$ and $\Delta\Omega^\dagger_{WC} \equiv \Omega_{\text{ts}} - \Omega_W$, respectively. According to the transition state theory[20], the mean first passage time between transitions from one minimum to the other depends exponentially on the free energy barrier:

$$\tau(P, T) = \tau_0 \exp\left(\frac{\Delta\Omega^\dagger(P, T)}{k_B T}\right) . \qquad (2)$$

Summing up, the stability of a given state and the kinetics of the transition to another state are ruled by the free energy landscape through Equation (1) and (2).

Rare events techniques[21] have been developed in order to compute $p(z; P, T)$ on complex free energy landscapes overcoming the extremely different timescales involved. Here we employ *restrained molecular dynamics* (RMD, adapted from Ref.[22]), which has been shown to be effective in dealing with superhydrophobicity (see Ref.[17,23] and *Supporting Information*). The advantage of using an atomistic description of the surface and of the liquid is that it relies on minimal assumptions. Furthermore the dimensions of the simulated system ~ 5 nm

are sufficiently large so that it can be described in terms of macroscopic capillarity[8,24] (see below); comparing atomistic and macroscopic models makes it possible to draw conclusions from the nano to the macro scale.

The salient features of the Salvinia – re-entrant geometry and heterogeneous chemistry – are captured in the simulations by a T-shaped cavity, resembling that found in experiments[6] and simulations[25], but with a hydrophilic top layer (contact angle $\theta_{\text{top}} = 55°$) combined with a hydrophobic interior ($\theta_{\text{in}} = 110°$, see Figure 1b). To disentangle the effect of the geometry from that of the chemistry we also simulate a purely hydrophobic surface ($\theta_{\text{in}} = \theta_{\text{top}} = 110°$) and a purely hydrophilic one ($\theta_{\text{in}} = \theta_{\text{top}} = 55°$) with the same T shape.

RMD simulations are run at constant pressure and temperature for Lennard-Jones fluid and solids (see *Supporting Information*). The free energy profiles thus obtained are reported in Figure 1c as a function of the filling fraction Φ of the cavity for zero pressure difference $\Delta P \equiv P_l - P_v - P_g \approx 0$, where P_l, P_v, and P_g are the pressures in the liquid, vapor, and gas phases. The filling fraction is defined as $\Phi \equiv (z_W - z)/(z_W - z_C)$, where z_W and z_C are the number of atoms inside the yellow box of Figure 1b corresponding to the Wenzel and to the Cassie state, respectively.

At $\Delta P \approx 0$, the free energy profiles for the three chemistries exhibit two minima which correspond to the Wenzel and Cassie states. At negative ΔP a third metastable state emerges at large Φ, corresponding to the evaporated state. Figure 1c shows that the Salvinia-like free energy profiles (red) are, to a good approximation, a superimposition of the hydrophobic (in green, for $0 < \Phi < 1$) and the hydrophilic ones (in blue, for $\Phi > 1$). This explains the essential function of the heterogeneous structure of the Salvinia: the hydrophobic interior *stabilizes the Cassie state* with respect to liquid intrusion (Cassie-Wenzel transition), while the hydrophilic top *hinders gas nucleation* (details in the following). This is our main result, which at the same time clarifies in quantitative terms the function of a complex biological structure, first described by Barthlott and coworkers[4], and suggests how to exploit it in the design of simpler bioinspired
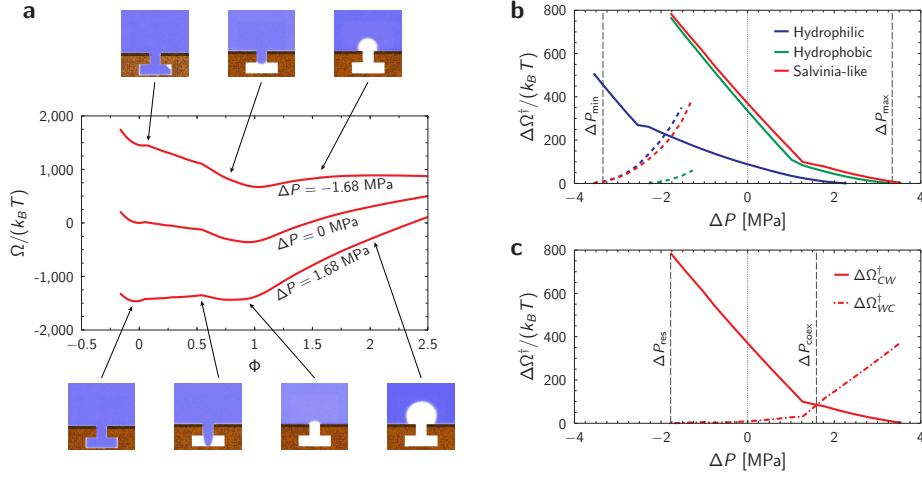
5

Figure 2: a) Free energy profiles for the Salvinia-like structure at different pressures; an arbitrary vertical shift is added for clarity. The insets show the most probable configurations along the transition. b) Free energy barriers as a function of pressure for the three systems as computed from RMD simulations. Solid lines are used for $\Delta\Omega^\dagger_{CW}$ and dashed ones for $\Delta\Omega^\dagger_{Cv}$. The vertical lines are the macroscopic estimates for the spinodal pressures $\Delta P_{\max} = 2\gamma_{lv}/w$ and $\Delta P_{\min} = -2\gamma_{lv}/w$. c) Cassie-Wenzel (solid) and Wenzel-Cassie (dashed-dotted) free energy barriers as a function of pressure for the Salvinia-like structure. ΔP_{res} is the spinodal pressure at which the Cassie state is spontaneously restored from the Wenzel one; ΔP_{coex} is the coexistence pressure where the Cassie and Wenzel states are equiprobable (same free energy).

surfaces.

Figure 2a addresses the effect of the pressure on the free energy profiles, which amounts to adding to $\Omega(\Phi)$ a term $\sim \Phi\Delta P$[18,24]; this linear shift changes the location of the minima and determines the stability of the Cassie state: for instance, increasing the pressure always favors the Wenzel state. At sufficiently large pressures, the Cassie minimum disappears and $\Delta\Omega^\dagger_{CW} \to 0$: this is the *spinodal* pressure $\Delta P_{\max}$ for the Cassie-Wenzel transition, i.e., the maximum pressure before the mechanical destabilisation of superhydrophobicity (mechanism 1). At $\Delta P < 0$ ("negative pressures") vapor bubbles tend to nucleate from the T structure ("cavitation"). The thermodynamically stable vapor state is separated from the Cassie state by the free energy barrier $\Delta\Omega^\dagger_{Cv}$.

Figure 2b reports $\Delta\Omega^\dagger_{CW}$ and $\Delta\Omega^\dagger_{Cv}$ as a function of pressure for the three chemistries considered. The barriers are typically hundreds of $k_B T$, accounting

6

for experimentally relevant metastabilities. Cavitation is favored by extreme negative pressures, which cause a reduction of $\Delta\Omega^\dagger_{Cv}$; this barrier vanishes at the Cassie-vapor spinodal pressure $\Delta P_{\min}$ where the Cassie minimum disappears (mechanism 4). The chemistry of the *top layer* determines $\Delta\Omega^\dagger_{Cv}$, with the hydrophilic one having a much larger barrier for cavitation (Salvinia effect). On the other hand, $\Delta\Omega^\dagger_{CW}$ is large at negative pressures and monotonically decreases with ΔP; its value depends on the chemistry of the interior of the cavity, with the hydrophobic one having the largest intrusion barrier.

Figure 2c reports the backward Wenzel-Cassie barrier $\Delta\Omega^\dagger_{WC}$. It is seen that the Cassie state can be *rest*ored at pressures below the Wenzel-Cassie spinodal, ΔP_{res}, where $\Delta\Omega^\dagger_{WC} \to 0$. This result, which is not captured by the macroscopic capillarity theory[18], shows that the Wenzel state can be "reversible", suggesting that superhydrophobicity can be restored, albeit at negative ΔP.

In the following, we go beyond the atomistic scale and derive design principles of general validity for superhydrophobic submerged surfaces. Using the concepts of classical capillarity, we first focus on the conditions of existence of the superhydrophobic Cassie state and how these are affected by the chemistry and topography of the surface texturing. Then, we show how the Salvinia-like structure is able to extend the range of pressures where superhydrophobicity is stable. The atomistic "experiment" and continuum models are in qualitative agreement, confirming the general validity of our design principles.

For the T geometry, the suspended state is attained at the corners of the solid surface or at the chemical contrast, which allow the *pinning* of the contact line, Figure 3a. In macroscopic terms this corresponds to the so-called Gibbs' criterion[26], which prescribes that the range of possible contact angles β (Fig. 1b) at a sharp corner or at a chemical contrast be included between the Young's angles approaching the discontinuity from the two sides. On the T

structure this pinning interval is

$$\phi_1 + \theta_{\text{top}} - 180° < \beta < \theta_{\text{in}} \tag{3a}$$

$$\theta_{\text{in}} < \beta < 180° - \phi_2 + \theta_{\text{in}} \tag{3b}$$

with Equation (3a) referring to the top corners/chemical contrast and Equation (3b) to the re-entrant ones (for the definitions, see Figure 1b; for an extended discussion, see the *Supporting Information*).

From a mechanistic point of view, in the generic case of a periodic pattern of macroscopic structures, the force balance at the Cassie state is given by (see, e.g., Ref. [8]):

$$\Delta P = -2\gamma_{lv} \cos \beta \, \frac{L}{A_{\text{mouth}}} \tag{4}$$

where γ_{lv} is the liquid-vapor surface tension, L is the length of the contact line, and A_{mouth} is the liquid-vapor area projected on the horizontal plane. For the T structure $L/A_{\text{mouth}} = 1/w$ with w the width of the cavity mouth; furthermore, the angle β is limited by Equation (3), which, together with Equation (4), dictates the range of pressures where the Cassie state exists: the minimum possible pressure is $\Delta P_{\min} \equiv \min_{\cos \beta} (-2\gamma_{lv} \cos \beta \, L/A_{\text{mouth}})$, while the maximum is $\Delta P_{\max} \equiv \max_{\cos \beta} (-2\gamma_{lv} \cos \beta \, L/A_{\text{mouth}})$. $\Delta P_{\min}$ and $\Delta P_{\max}$ are the spinodal pressures for the Cassie state: for $\Delta P \leq \Delta P_{\min}$ the system cavitates while for $\Delta P \geq \Delta P_{\max}$ the liquid intrudes the cavities toward the Wenzel state.

For the Salvinia-like structure the intrusion and nucleation spinodals are attained at $\beta_{\max} = 180°$ and $\beta_{\min} = 0°$ which plugged into Equation (4) yield $\Delta P_{\max} = 2\gamma_{lv}/w$ and $\Delta P_{\min} = -2\gamma_{lv}/w$, respectively. A crucial feature of the Salvinia-like structure, therefore, is that both spinodals are not explicitly dependent on the chemistry of the surface; the chemistry, together with the re-entrant topography of the surface, only ensures that $\beta_{\max} = 180°$ and $\beta_{\min} = 0°$ are within the pinning interval of Equation (3). Importantly, these values also maximize the range of pressures where the superhydrophobic state exists for a given w. In the chemically homogeneous cases, instead, this pressure range is
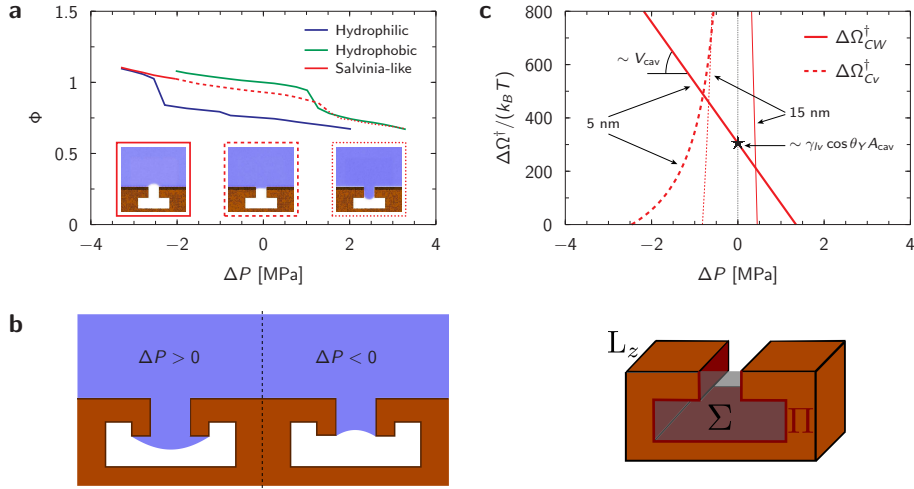
Figure 3: a) Filling level Φ at the Cassie minima of the free energy as a function of the pressure as computed from RMD. The Salvinia-like structure presents three different pinning regimes (insets): at the top corners ($\Delta P < 0$), at the chemical contrast ($\Delta P \sim 0$), and at the lower corners ($\Delta P > 0$). b) Sketch of the serif T geometry, which can prevent intrusion even for liquids with low contact angles ($\theta_{in} = \theta_{top} \approx 0$). c) Intrusion and nucleation free energy barriers as computed via approximate macroscopic expressions (see *Supporting Information*). $\Delta\Omega^{\dagger}_{CW}$ (solid lines) and $\Delta\Omega^{\dagger}_{Cv}$ (dashed lines) are plotted for two systems with reference dimensions $w = 5$ nm (thick lines) and $w = 15$ nm (thin lines). The volume of the cavity is given by $V_{cav} = \Sigma L_z$ and its internal area by $A_{cav} = \Pi L_z$. For the intrusion barrier we assume $\Delta\Omega^{\dagger}_{CW} \approx -3\Delta P V_{cav}/4 - 7\gamma_{lv}\cos\theta_{in}A_{cav}/9$; for the nucleation barrier $\Delta\Omega^{\dagger}_{Cv} \approx \pi\gamma_{lv}^2 L_z/|\Delta P| - 2\gamma_{lv}wL_z$.

smaller and explicitly depends on the chemistry (see *Supporting Information*).

Summarizing, in order to realise these optimal conditions for submerged superhydrophobicity, the geometry of the cavity mouth should be combined with the chemistry in such a way that $180° - \phi_2 + \theta_{in} \geq 180°$ and $\phi_1 + \theta_{top} - 180° \leq 0°$. More complex geometries, such as the doubly re-entrant "serif T" ($\phi_1 = 90°$ and $\phi_2 \approx 0°$) [27], can be designed in order to repel liquids with low contact angles ($\theta_{in} = \theta_{top} \approx 0°$) [28]. In this case, the meniscus is pinned at the innermost corner for $\Delta P > 0$ (see Figure 3b and *Supporting Information*).

Based on Equation (1) and (2) we now discuss the stability of submerged superhydrophobicity. As compared to drop-repellent surfaces, typical submerged applications require the superhydrophobic state to survive for longer times and

9

at comparatively larger pressures. The thermodynamic stability of the Cassie state – i.e., Cassie being the absolute minimum of $\Omega(\Phi; P, T)$ – is often invoked in order to obtain such "robust" superhydrophobicity. This criterion usually requires overly tall and fragile structures and is redundant since the duration $\tau(P, T)$ of a metastable Cassie state is typically much larger than the experimental timescale. For our Salvinia-like nanostructure, Equation (2) – assuming (conservatively) molecular timescales for the prefactor[20], $\tau_0 = h/(k_B T) \approx 10^{-13}$ s, where h is Planck's constant, and $\Delta\Omega^\dagger \sim 100\ k_B T$ (Fig. 2b) – predicts that the lifetime of the Cassie state exceeds the age of the universe. In other words, if the free energy barriers are sufficiently large the superhydrophobic state – stable or metastable – is robust and mechanisms 2 and 3 of gas loss are in practice inhibited.

The typical trend of the free energy barriers with the characteristic size w of the surface texturing is shown in Figure 3c: increasing the size of the cavity decreases $\Delta P_{\max}$ and dramatically increases the dependence of $\Delta\Omega^\dagger_{CW}$ on ΔP; the effect on cavitation is similar. Thus, the thermally activated breakdown of superhydrophobicity (mechanisms 2 and 3 of gas loss) becomes important only in the vicinity of the spinodals, where the barrier is of the order of the thermal energy $k_B T$. The amplitude of this region rapidly shrinks with the size of the structures (see Figure 3c).

In summary, atomistic rare events simulations have shown what are the essential features of the Salvinia effect: a re-entrant geometry, together with a hydrophobic interior, improves the stability of gas pockets against liquid intrusion and contaminants, while the hydrophilic top surface hinders the nucleation and coalescence of bubbles. This natural paradigm reveals two simple design principles for engineering submerged surfaces: the pinning interval can be tuned via the chemistry and surface topography (Equation (3)) and the range of positive and negative pressures where superhydrophobicity is (meta)stable can be controlled via the size of the cavity mouth (spinodal pressures). Smaller structures typically correspond to larger superhydrophobic pressure ranges; however,

the range of pressures over which the thermally activated breakdown of super-hydrophobicity is possible broadens for smaller structures, eventually limiting this "shrinking" strategy.

Acknowledgements

References

[1] W. Barthlott, C. Neinhuis. *Planta* **1997**, *202*, 1 1.

[2] X. Zhang, F. Shi, J. Niu, Y. Jiang, Z. Wang. *J. Mater. Chem.* **2008**, *18*, 6 621.

[3] E. Celia, T. Darmanin, E. T. De Givenchy, S. Amigoni, F. Guittard. *J. Colloid Interface Sci.* **2013**, *402* 1.

[4] W. Barthlott, T. Schimmel, S. Wiersch, K. Koch, M. Brede, M. Barczewski, S. Walheim, A. Weis, A. Kaltenmaier, A. Leder, et al. *Adv. Mater.* **2010**, *22*, 21 2325.

[5] N. A. Patankar. *Langmuir* **2003**, *19*, 4 1249.

[6] A. Tuteja, W. Choi, M. Ma, J. M. Mabry, S. A. Mazzella, G. C. Rutledge, G. H. McKinley, R. E. Cohen. *Science* **2007**, *318*, 5856 1618.

[7] H.-J. Butt, C. Semprebon, P. Papadopoulos, D. Vollmer, M. Brinkmann, M. Ciccotti. *Soft Matter* **2013**, *9*, 2 418.

[8] A. Checco, B. M. Ocko, A. Rahman, C. T. Black, M. Tasinkevych, A. Giacomello, S. Dietrich. *Phys. Rev. Lett.* **2014**, *112*, 21 216101.

[9] P. Lv, Y. Xue, Y. Shi, H. Lin, H. Duan. *Phys. Rev. Lett.* **2014**, *112*, 19 196101.

[10] M. Xu, G. Sun, C.-J. Kim. *Phys. Rev. Lett.* **2014**, *113*, 13 136103.

[11] L. Joly, T. Biben. *Soft Matter* **2009**, *5*, 13 2549.

[12] J. P. Rothstein. *Annu. Rev. Fluid. Mech.* **2010**, *42* 89.

[13] D. Gentili, G. Bolognesi, A. Giacomello, M. Chinappi, C. Casciola. *Microfluid. Nanofluid.* **2014**, *16*, 6 1009.

[14] M. Schultz, J. Bendick, E. Holm, W. Hertel. *Biofouling* **2011**, *27*, 1 87.

[15] M. Ferrari, A. Benedetti. *Adv. Colloid Interface Sci.* **2015**, *doi:10.1016/j.cis.2015.01.005*.

[16] J. Hunt, B. Bhushan. *J. Colloid Interface Sci.* **2011**, *363*, 1 187.

[17] A. Giacomello, S. Meloni, M. Chinappi, C. M. Casciola. *Langmuir* **2012**, *28*, 29 10764.

[18] A. Giacomello, M. Chinappi, S. Meloni, C. M. Casciola. *Langmuir* **2013**, *29*, 48 14873.

[19] This transient case, which is beyond the goal of the paper, is observed, e.g., in surface nanobubbles or when a surface is initially immersed in a liquid.

[20] H. Eyring. *J. Chem. Phys.* **1935**, *3* 107.

[21] S. Bonella, S. Meloni, G. Ciccotti. *Eur. Phys. J. B* **2012**, *85*, 3 97.

[22] L. Maragliano, E. Vanden-Eijnden. *Chem. Phys. Lett.* **2006**, *426* 168.

[23] A. Giacomello, S. Meloni, M. Müller, C. M. Casciola. *J. Chem. Phys.* **2015**, *142*, 10 104701.

[24] A. Giacomello, M. Chinappi, S. Meloni, C. M. Casciola. *Phys. Rev. Lett.* **2012**, *109*, 22 226102.

[25] E. S. Savoy, F. A. Escobedo. *Langmuir* **2012**, *28*, 46 16080.

[26] J. Oliver, C. Huh, S. Mason. *J. Colloid Interface. Sci.* **1977**, *59*, 3 568.

[27] R. Hensel, R. Helbig, S. Aland, H.-G. Braun, A. Voigt, C. Neinhuis, C. Werner. *Langmuir* **2013**, *29*, 4 1100.

[28] T. Liu, C. Kim. *Science* **2014**, *346*, 6213 1096.